ISSN 1674-1056
http://cpb.iphy.ac.cn
http://iopscience.iop.org/cpb
中国物理 B
Chinese Physics
中国物理 Chinese Physics B

Epitaxially strained $SnTiO_3$ at finite temperatures

Dawei Wang(王大威), Laijun Liu(刘来君), Jia Liu(刘佳), Nan Zhang(张楠), Xiaoyong Wei(魏晓勇)

Citation: Chin. Phys. B . 2018, 27(12): 127702. **doi:** 10.1088/1674-1056/27/12/127702
Journal homepage: http://cpb.iphy.ac.cn; http://iopscience.iop.org/cpb

What follows is a list of articles you may be interested in

Electro-optical properties and (*E*, *T*) phase diagram of fluorinated chiral smectic liquid crystals

R Zgueb, H Dhaouadi, T Othman

Chin. Phys. B . 2018, 27(10): 107701. **doi:** 10.1088/1674-1056/27/10/107701

Calculation of electric field-temperature (*E*, *T*) phase diagram of a ferroelectric liquid crystal near the SmA-SmC_{α}^{*} transition

F Trabelsi, H Dhaouadi, O Riahi, T Othman

Chin. Phys. B . 2018, 27(3): 037701. **doi:** 10.1088/1674-1056/27/3/037701

Enhanced energy storage behaviors in free-standing antiferroelectric $Pb(Zr_{0.95}Ti_{0.05})O_3$ thin membranes

Zheng-Hu Zuo(左正笏), Qing-Feng Zhan(詹清峰), Bin Chen(陈斌), Hua-Li Yang(杨华礼), Yi-Wei Liu(刘宜伟), Lu-Ping Liu(刘鲁萍), Ya-Li Xie(谢亚丽), Run-Wei Li(李润伟)

Chin. Phys. B . 2016, 25(8): 087702. **doi:** 10.1088/1674-1056/25/8/087702

Realization of a flux-driven memtranstor at room temperature

Shi-Peng Shen(申世鹏), Da-Shan Shang(尚大山), Yi-Sheng Chai(柴一晟), Young Sun(孙阳)

Chin. Phys. B . 2016, 25(2): 027703. **doi:** 10.1088/1674-1056/25/2/027703

Composition and misfit strain dependence of electrocaloric effect of $Pb_{1-x}Sr_xTiO_3$ thin films

Qiu Jian-Hua, Ding Jian-Ning, Yuan Ning-Yi, Wang Xiu-Qin

Chin. Phys. B . 2013, 22(1): 017701. **doi:** 10.1088/1674-1056/22/1/017701

Epitaxially strained $SnTiO_3$ at finite temperatures*

Dawei Wang(王大威)[1,†], Laijun Liu(刘来君)[2,‡], Jia Liu(刘佳)[3], Nan Zhang(张楠)[4], and Xiaoyong Wei(魏晓勇)[4]

[1] School of Microelectronics and State Key Laboratory for Mechanical Behavior of Materials, Xi'an Jiaotong University, Xi'an 710049, China

[2] College of Materials Science and Engineering, Guilin University of Technology, Guilin 541004, China

[3] State Key Laboratory for Mechanical Behavior of Materials & School of Materials Science and Engineering, Xi'an Jiaotong University, Xi'an 710049, China

[4] Electronic Materials Research Laboratory–Key Laboratory of the Ministry of Education and International Center for Dielectric Research, Xi'an Jiaotong University, Xi'an 710049, China

(Received 14 August 2018; revised manuscript received 9 September 2018; published online 10 November 2018)

By combining the effective Hamiltonian approach and direct *ab initio* computation, we obtain the phase diagram of $SnTiO_3$ with respect to epitaxial strain and temperature. This demonstrates the complex features of the phase diagram and provides an insight into this system, which is a presumably simple perovskite. Two triple points, as shown in the phase diagram, may be exploited to achieve high-performance piezoelectric effects. Despite the inclusion of the degree of freedom related to oxygen octahedron tilting, the ferroelectric displacements dominate the structural phases over the whole misfit strain range. Finally, we show that $SnTiO_3$ can change from hard to soft ferroelectrics with the epitaxial strain.

Keywords: $SnTiO_3$, phase diagram, epitaxial strain

PACS: 77.80.–e, 77.84.–s, 81.30.Bx **DOI:** 10.1088/1674-1056/27/12/127702

1. Introduction

Piezoelectricity is a phenomenon in certain materials that strain and electric polarization can induce and/or influence each other. In response to an applied mechanical strain, ferroelectric materials, which are inherently piezoelectric, can produce an electric polarization proportional to the load. Similarly, these materials will produce a mechanical deformation (strain) in response to an applied voltage. Switchable polarization makes ferroelectrics a critical component in memories, actuators, electro-optic devices, and potential candidates for nanoelectronics.[1]

In recent years, it has been found that materials of high-performance piezoelectricity are often associated with morphortropic phase boundary (MPB), with examples including $Pb(Zr,Ti)O_3$[2] and $(K,Na)NbO_3$-$LiTaO_3$-$LiSbO_3$,[3] or triple points, such as in $(Ba,Ca)(Zr,Ti)O_3$.[4] Engineering solid solutions to a certain composition can create phase boundaries and tricritical points, where the crystal structure changes abruptly, inducing maximal piezoelectric properties. Three important situations have been extensively studied: (i) MPB in pure perovksites that separates regions of the tetragonal from the rhombohedral symmetry;[5] (ii) MPB formed in perovskites dissoluted with a small amount of non-perovskite-structured materials that can cause lattice distortions,[3] and grain boundary effects;[6] and (iii) regions close to a triple point where cubic paraelectric phase (C), ferroelectric rhombohedral (R), and tetragonal (T) phases meet.[4] In addition to MPB, epitaxial thin-film growth, which introduces intrinsic lattice strain, has matured as another important method to design desired ferroelectric materials, which is important for highly integrated design and intelligent control technology.[7,8] Strain engineering is widely adopted and can tune the large 2p–3d charge hybridization between the strongly correlated 3d electrons in transition metal ions and the 2p electrons of oxygens.[9–12] For instance, both compressive and tensile strains increase the Ni 3d band width and favor the metallic phase in $NdNiO_3$.[13] In addition, substrate clamping will force the temperature dependence of in-plane lattice constants to follow that of the substrates, which may lead to unexpected phase transitions and domain formation.[14,15] Therefore, strain constraint can introduce muti-phase coexistence in thin films, which makes it an attractive method to fine tuning film properties.

Nowadays, the commonly used high-performance piezoelectric materials, including $PbTiO_3$ and $Pb(Mn,Nb)O_3$, contain hazardous lead (Pb). Since Pb is harmful to environment and human health, lead-free ferroelectric materials are highly desired. Many lead-free materials are based on $(Bi_{0.5},Na_{0.5})TiO_3$, $(K,Na)NbO_3$ or $BaTiO_3$; however, their performance is still sub-optimal compared to Pb-containing materials.[16] Since Sn and Pb belong to the same family, $SnTiO_3$ is expected to achieve high-performance piezoelectricity with environmentally benign elements.[17,18] Indeed,

*Project supported by the National Natural Science Foundation of China (Grant Nos. 11574246, 51390472, U1537210, and 11564010), the National Basic Research Program of China (Grant No. 2015CB654903), the Natural Science Foundation of Guangxi Zhuang Autonomous Region (Grant Nos. GA139008 and AA138162), and the "111" Project of China (Grant No. B14040).

†Corresponding author. E-mail: dawei.wang@mail.xjtu.edu.edu

‡Corresponding author. E-mail: 2009011@glut.edu.edu

© 2018 Chinese Physical Society and IOP Publishing Ltd

$SnTiO_3$ has large polarization and large axial ratio,[19,20] even larger than $PbTiO_3$, making it a promising candidate. But for various reasons, $SnTiO_3$ bulk material is hard to prepare because Sn^{2+} can easily become Sn^{4+}, and Sn is prone to enter into the B site (where the Ti ion stays) due to its small ionic radius. However, researchers continued to look for opportunities to exploit the remarkable properties of $SnTiO_3$. For instance, researchers have considered Sn-doped $BaTiO_3$,[21,22] Bennett *et al.* considered $Sn(Al_{0.5},Nb_{0.5})O_3$,[23] while Suzuki *et al.* obtained Sn-doped $SrTiO_3$,[24] and Laurita investigated (Sr,Sn)TiO_3 and (Ba,Ca,Sn)TiO_3.[25] Recently, Agarwal *et al.*[26] obtained perovskite phase $SnTiO_3$ with the atomic-layer deposition technique. This is an important breakthrough that will excite more work on $SnTiO_3$.

In addition to experimental work, there are also many theoretical investigations of $SnTiO_3$.[17–19,27–31] However, most of previous theoretical investigations are based on direct *ab initio* computation, which cannot provide information regarding $SnTiO_3$ at finite temperatures. Therefore, many important questions remain unanswered. For instance, what are the conditions for the existence of different ferroelectric phases? What does the phase diagram of $SnTiO_3$ look like? Can such a seemingly simple perovskite ($SnTiO_3$ is not a solid solution and no doping is applied) possess complex features? In this work, we will focus on the finite temperature properties of epitaxially strained $SnTiO_3$ and address these questions. We note that this information will be useful for the fabrication of $SnTiO_3$ bulk, or the growth of $SnTiO_3$ film, and engineering $SnTiO_3$-containing ferroelectric materials. Since $SnTiO_3$ bulk is not available, there is little *a priori* information at finite temperatures that can be used in this work. While our computational results are less convincing without the support from experiments, it demonstrates the value of theoretical and numerical work — *i.e.*, their power to predict something unknown — and this is one of the reasons that motivated this investigation.

2. Method

To fully understand $SnTiO_3$, it is necessary to know all of its possible phases under various conditions. However, it is not trivial to achieve this goal. For instance, the direct *ab initio* approach usually provides us with the structural phase of local energy minimum (in contrast to the most stable phase of global energy minimum), which is exacerbated by the 0-K assumption adopted. The application of this approach often requires a comparison of many different phases that may not be able to cover all possibilities. To address this problem, here we adopt the first-principles based effective Hamiltonian approach and Monte–Carlo (MC) simulations, which were developed exactly to address these challenges. To use this approach, it is necessary to compute tens of coefficients appearing in the effective Hamiltonian using direct *ab initio* computation before carrying out MC simulations.

The effective Hamiltonian used here was originally developed in Refs. [32] and [33], which incorporate the coupled dynamics of the soft mode, strain, and dipole. Its internal energy is given by

$$E = E^{\mathrm{FE}}\left(\{\boldsymbol{u}_i\},\{\boldsymbol{v}_i\},\eta_{\mathrm{H}}\right), \tag{1}$$

where $\boldsymbol{u}_i$ is the local soft-mode in unit cell i, and is proportional to the local electric dipole moment in that cell when multiplied by Born effective charge. We note that $\boldsymbol{u}_i$ here is located on the A-site (where Sn stays), and represents the collective motion of Sn, Ti, and O atoms inside one unit cell. The $\boldsymbol{v}_i$ are Sn-centered local displacements related to the inhomogeneous strain inside each unit cell. η_{H} is the homogeneous strain tensor. The energy terms and associated parameters can be found in Refs. [32], [33], and [34]. In this work, we extended the effective Hamiltonian and expanded the local energy term to 8th order (similar to Ref. [35]) to describe the internal energy more precisely.[36] In addition, the antiferrodistortive (AFD) oxygen octahedron tilting is also considered with the energy term[37]

$$E = E^{\mathrm{AFD}}\left(\{\boldsymbol{\omega}_i\},\{\boldsymbol{u}_i\},\{\boldsymbol{v}_i\},\eta_H\right), \tag{2}$$

where the new variable $\boldsymbol{\omega}_i$ represents the oxygen tilting on the unit cell i, which centers on the B-site atom (*i.e.*, Ti). The pristine expression of E^{AFD} can be found in Ref. [37], which also includes the couplings between AFD, and all the other dynamical variables. The associated parameters in E^{AFD} are obtained in a similar way as in Ref. [34]. The effective Hamiltonian approach is a well established methodology that has been developed since 1994[32,33,38] and similar to direct *ab initio* methods, it has been used in many investigations, *e.g.*, to predict new structural phases of perovksites.[39,40] The most appealing features of this approach are the following: (i) it can often lead us to the most stable structural phase of global energy minimum; and (ii) it can produce finite temperature properties, which explains why we adopt this approach in our work.

With the effective Hamiltonian, we perform MC simulations on a $12\times12\times12$ supercell, containing 8640 atoms. The system is set to meet the periodic boundary condition along the (pseudo) x,y,z directions and subject to various epitaxial strains. In each simulation at a given epitaxial misfit strain s, we gradually cool down the system from 2500 K to 5 K. For each temperature, we carry out 1.6×10^5 MC steps to obtain averaged physical quantities, most importantly the supercell average of local mode, which can be used to determine the symmetry of the system and the approximate positions of each atom in it. The use of supercell is necessary to find various possible structural phases and accurate phase transition temperatures. For instance, to simulate antiferroelectric perovksites, at least two primitive unit cells are needed. Similarly,

for AFD related phases, two or more primitive unit cells are necessary. In fact, the ability to simulate large supercells is an important feature and advantage of the effective Hamiltonian approach, which enables us to find the energy ground state.

In this approach, the symmetries or temperatures are not preset in the effective Hamiltonian. The starting point of the effective Hamiltonian is the cubic phase ($Pm\bar{3}m$), which is used as the reference state. The effective Hamiltonian quantifies the energy change when ion displacements and deformation (*i.e.*, strain) happen with respect to this reference state. This energy change is then used in the MC simulations to find the averaged ion displacements and deformation at a given temperature (and epitaxial strain). Finally, the ion displacements and the deformation are used to determine the structural phase (and symmetry) of $SnTiO_3$ at the given temperature. In this process, the temperature is a given parameter for each MC simulation, which employs the effective Hamiltonian and the symmetry of $SnTiO_3$ is inferred after the MC simulation is done.

We have also performed direct *ab initio* computation to corroborate MC simulation results. For this purpose, the open source ABINIT software package[41] is used along with the local density approximation (LDA)[42] and the projector-augmented-wave (PAW) method.[43] We use the pseudopotentials implemented in the GBRV package,[44] and the Sn 4d 5s 5p, Ti 3s 3p 4s 3d, and O 2s 2p orbitals are treated as valence orbitals. For convergence, we have chosen the cut-off energy (`ecut`) to be 25 Hartree (1 Hartree = 27.211 eV) for plane wave expansion, and the fine grid cut-off energy (`pawcutdg`) is selected to be 50 Hartree. In addition, k-point sampling of $6\times6\times6$ Monkhorst–Pack grid[45] was used. The atomic coordinates are relaxed until all atomic-force components are smaller than 10^{-5} Hatree/Bohr, and the cell size and shape are varied until all stress components are below 10^{-7} Hatree/Bohr^3.

Both the MC simulations and the direct *ab initio* computations deal with the strained bulks (in contrast to ultrathin two-dimensional films) given the periodic boundary condition used. However, many properties of the strained films (as long as they are not just a few atomic layers thick) can be inferred from these calculations. Comparing to our previous work,[34] the present investigation develops in three directions:

i) We now include the new degree of freedom, *i.e.*, oxygen octahedron tilting (often called antiferrodistortive rotations, AFD), which is ignored in the previous work.[34]

ii) To this end, we computed many new essential parameters for the effective Hamiltonian. While the current work build on the previous one, it has substantially extended the effort to fully simulate $SnTiO_3$.

iii) Here we consider the effects of epitaxial strain and show that $SnTiO_3$ has a rather complex phase diagram, containing interesting phase boundaries and triple points.

3. Results

To obtain the phase diagram, we have performed MC simulations for misfit strain between $s = 0$ and $s = 2\%$ with a step size of $\Delta s = 0.125\%$. For each misfit strain s, the system is gradually cooled down from ~ 2500 K to 5 K and its evolution with temperature is observed. The simulation results are then summarized to form the phase diagram.

3.1. Phase transition and phase diagram

We first obtain the supercell averaged local mode *versus* temperature of $SnTiO_3$ under various tensile epitaxial strains, which is expected to stabilize $SnTiO_3$.[20] This information enables us to find the evolution of structural phases with respect to temperature and epitaxial strain, and more importantly, the phase transition temperatures of the system. Figure 1 shows the results with misfit strain s =0.375% and s =1%. Note that we have relaxed the cubic phase ($Pm\bar{3}m$) $SnTiO_3$ using ABINIT (with settings specified in Section 2) to obtain the lattice parameter $a = 7.312$ Bohr, which is used as the reference value for specifying the misfit strain.

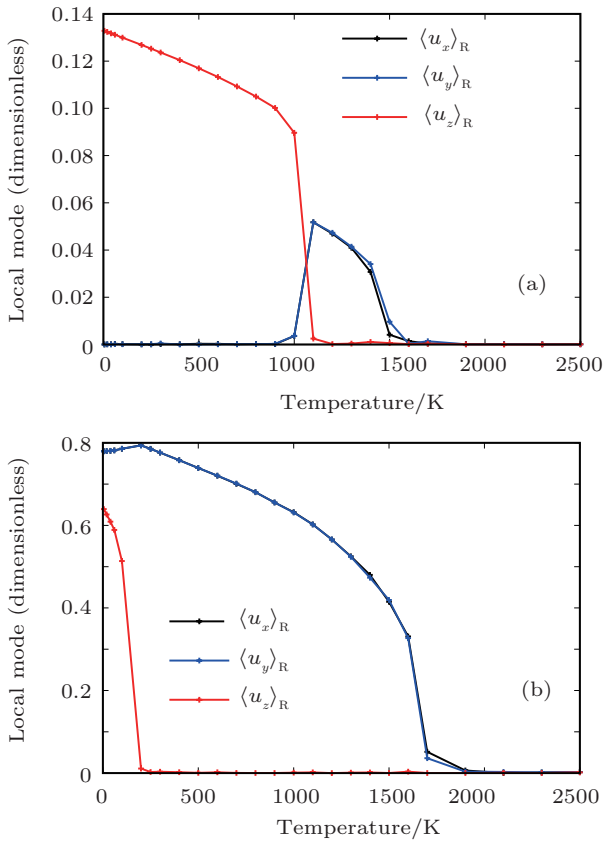


Fig. 1. (color online) Local mode *versus* temperature at two given strain misfit, s =0.375% (a) and s =1% (b).

For the smaller epitaxial strain $s = 0.375\%$, the system adopts $P4mm$ phase for temperature $T \lesssim 1000$ K, ($P_x = P_y = 0$, $P_z > 0$), as the temperature increases it undergoes a phase transition to become the $Amm2$ phase ($P_x = P_y > 0$, $P_z = 0$), and

eventually the cubic phase for $T \gtrsim 1500$ K. The whole process is somewhat similar to that of $BaTiO_3$ and $(Na_{0.5},K_{0.5})NbO_3$, where several structural phases are involved in phase transitions. Here, however, a rather drastic change happens at around 1000 K as the polarization rotates from out-of-plane to the in-plane configuration. For the larger epitaxial strain ($s = 1\%$), there are also two phase transitions. At low temperature ($T \lesssim 197$ K), it adopts the *Cm* ($P_x = P_y > 0, P_z > 0$) phase, which changes to the *Amm*2 phase as the temperature increases, and finally becomes paraelectric at $T \simeq 1750$ K. This phase transition temperature is high comparing to other typical ferroelectric materials, *e.g.*, $PbTiO_3$ (763 K) and $BiFeO_3$ (1100 K).[46] This is likely due to the strong dipole–dipole interaction inside $SnTiO_3$, noting that the spontaneous polarization of $SnTiO_3$ (1.32 C/m^2)[34] is even larger than the strained $BiFeO_3$ (1.30 C/m^2).[47] Given the high phase transition temperatures, we note that in the MC simulations $SnTiO_3$ is assumed to be always in the solid state (*i.e.*, it is not melted) when the structural phases are obtained. While the melting point of $SnTiO_3$ is not yet available experimentally, it is likely lower than that of $PbTiO_3$, which is 1554 K.

No correlated AFD was observed for the epitaxial strains investigated here, which is consistent with previous known results[20] (also see Section 4). Figure 1 indicates that four phases (paraelectric $Pm\bar{3}m$, orthorhombic *Amm*2, tetragonal *P*4*mm*, and monoclinic *Cm*) can all exist in $SnTiO_3$ at proper temperature and epitaxial strain. Without strain constraint or at tiny strain ($s < 0.5\%$, see Fig. 2), the system adopts the *P*4*mm* phase ($P_z > 0$, $P_{x,y} = 0$) at low temperature, and only has one phase transition (*P*4*mm* to paraelectric) as temperature increases. Interestingly, figure 1(b) shows a region ($T \leq 200$ K) that corresponds to the M_B phase (belong to space group *Cm*),[36,38] and for smaller s (*e.g.*, at $s = 0.75\%$), we have observed that $P_z > P_x = P_y$, which is also *Cm*, but corresponds to the M_A phase.[48] Moreover, in Fig. 1(a), both the M_A and M_B phases exist between the T (*P*4*mm*) and O (*Amm*2) phases. The phase transition sequence resembles the local structure evolution of $Pb(Ti_{1-x}, Zr_x)O_3$ with increasing x.[49] This monoclinic region has been shown to play critical role in high-performance piezoelectric materials.[50]

We now turn to the phase diagram of $SnTiO_3$ with respect to temperature and epitaxial strain. First, for all the investigated misfit strains (up to 2%), figure 2 shows that $SnTiO_3$ undergoes a paraelectric to ferroelectric phase transition at rather high temperature ($T_C > 1400$ K). The high T_C is likely due to the large intrinsic spontaneous polarization discussed previously.[34] Second, T_C initially decreases with s, reaching a minimum, and then increases again.[51] The lowest point corresponds to a triple point separating the paraelectric phase and the other two ferroelectric phases (tetragonal *P*4*mm* and orthorhombic *Amm*2), similar to what happens in ultrathin $PbTiO_3$ films.[15] We note that the existence of the *Cm* phase is consistent with results obtained in Ref. [20]. The abrupt transition from the *P*4*mm* to the *Cm* phase (with respect to the misfit strain) happens in a slender region ($< 0.125\%$) represented by a straight line in Fig. 2 due to the limit of Δs used in simulations.

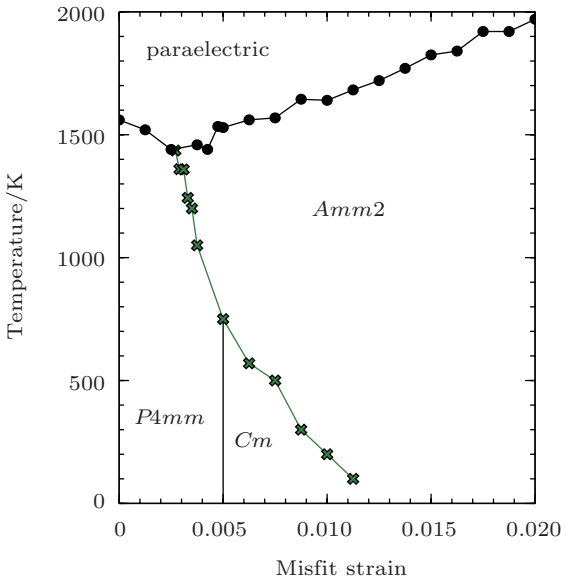


Fig. 2. Phase diagram of epitaxially strained $SnTiO_3$.

The first triple point in Fig. 2, where one paraelectric cubic phase and two ferroelectric phases converge, contains potential large piezoelectric effects. For instance, a triple point was found and exploited in binary compounds including $(Ba_{0.7},Ca_{0.3})TiO_3$-$Ba(Zr_{0.2},Ti_{0.8})O_3$ (BCZT),[4] $Ba(Sn_{0.12},Ti_{0.88})O_{3-x}(Ba_{0.7},Ca_{0.3})O_3$,[52] and other $BaTiO_3$-derived systems.[53] More importantly, the three ferroelectric phases (*P*4*mm*, *Amm*2, and *Cm*) converge to a second triple point. There are three boundaries around this point. The boundary at $s = 0.5\%$ separates the *P*4*mm* and the *Cm* phase, resembling the MPB seen in $Pb(Zr_{1-x}, Ti_x)O_3$, in which two different structural phases exist with a buffer region at $x \simeq 0.48$. In $Pb(Zr_{1-x}, Ti_x)O_3$ the monoclinic phase serves as a bridge between the higher symmetry tetragonal phase (with [001] polarization) and the rhombohedral phases (with [111] polarization).[37] In this connecting phase, the polarization can align anywhere on the {110} mirror plane between the pesudocubic [111] and [001] directions, giving rise to the high piezoelectric response.[37,54,55]

Here in $SnTiO_3$, the pronounced existence of the *Cm* phase and the second triple point, which bridges the tetragonal phase (with [001] polarization) and the orthorhombic phase (with [110] polarization), may also enable high performance, following the pattern of the universal phase diagram discussed in Refs. [54] and [55]. The reason is similar to that of $Pb(Zr_{1-x}, Ti_x)O_3$: in this region, polarization anisotropy nearly vanishes and thus polarization rotations are easy.[48] Many alkaline niobate perovskites show a polymorphic phase

transition [56] between the tetragonal phase and the orthorhombic phase, similar to what happens in Fig. 2. The polymorphic behavior can also lead to high piezoelectricity due to the instability with respect to polarization rotation.[57] However, the temperature stability of their piezoelectric properties for alkaline niobate perovskites is not as good as $Pb(Zr_{1-x},Ti_x)O_3$. In addition, the large anisotropy along the whole polymorphic boundary line leads to a larger energy barrier between the two polarization states (tetragonal and orthorhombic), preventing possible polarization rotations because the phase coexistence results from the diffusive tetragonal to orthorhombic phase transformation.[4] In $SnTiO_3$, unlike the polymorphic phase transition, the *Cm* phase is associated with a triple point, where a low energy barrier between two ferroelectric phases (*P*4*mm* and *Amm*2) may exist that facilitates the polarization rotation and lattice distortion, leading to high performance. Unfortunately, this triple point is not at room temperature for pure $SnTiO_3$ (which is at $\sim$ 750 K as shown in Fig. 2), and may need to be tuned (*e.g.* by doping). For instance, following the lessons from BCZT, it may be possible to use Pb to substitute Sn and/or Zr to substitute Ti. In this way, $SnTiO_3$ can be taken as the matrix material for designing high performance piezoelectric materials.

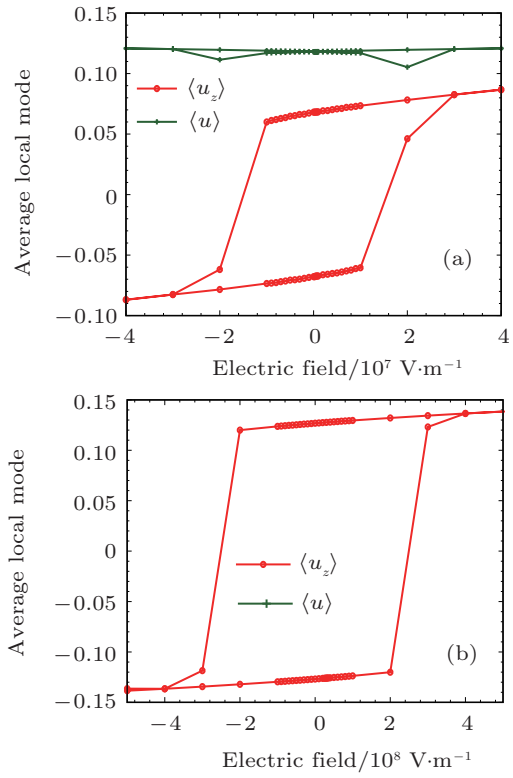


Fig. 3. (color online) Hysteresis loop of $SnTiO_3$ at $s = 0.75\%$ (a) and $s = 0\%$ (b) at 300 K. The electric field is applied along the z axis.

To show that the polarization in the *Cm* phase can easily rotate, we also obtained the hysteresis loop at different epitaxial strains. As figure 3 shows, the *Cm* phase has a strong effect on the hysteresis loop of $SnTiO_3$. When the *Cm* phase exists [Fig. 3(a)] at $s = 0.75\%$, the coercive field is $\sim 1.6 \times 10^7$ V/m, reduced by a factor of 10 compared to the result obtained when $s = 0\%$ ($> 2 \times 10^8$ V/m, see Fig. 3(b)). Analogous to magnetic materials, by applying a proper strain (*e.g.*, 0.75%), $SnTiO_3$ becomes "soft" ferroelectrics. Interestingly, in the whole process, the magnitude of the polarization $\boldsymbol{P}$ is approximately a constant [dark green line in Fig. 3], making the whole process a rotation as well as switching of polarization (albeit a sudden rotation), consistent with previous computations.[30,31]

3.2. Direct *ab initio* computation

To corroborate the results obtained from effective Hamiltonian-based computations, we also obtained numerical results from direct *ab initio* computation.

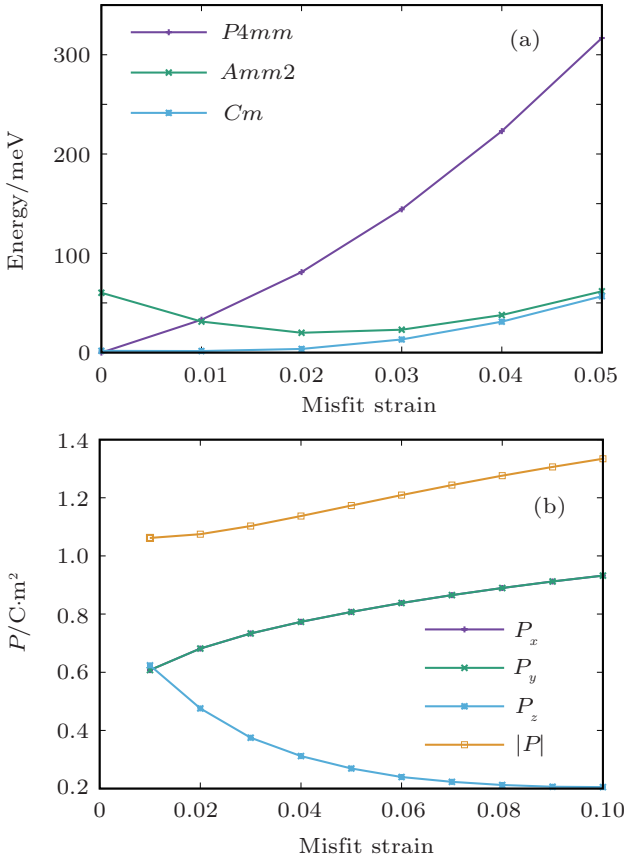


Fig. 4. (color online) (a) Energy and polarization *versus* strain for three different phases *Amm*2, *P*4*mm*, and *Cm*. At $s = 0\%$; (b) The polarization ($P_x = P_y$ and P_z) *versus* strain for the *Cm* phase.

Figure 4(a) shows the energy *versus* strain for the *P*4*mm*, *Amm*2, and *Cm* phases. These phases all appear in the phase diagram of $SnTiO_3$ (Fig. 2). For a large range of epitaxial strain, the *Cm* phase has the lowest energy. At $s = 1\%$, the energy of the *Cm* phase is approximately 29.4 meV lower than that of *P*4*mm* or *Amm*2. These results indicate that the *Cm* phase can be the ground state for a restricted range of strain, which supports our effective Hamiltonian results. The *Cm* phase appears around $s = 0.5\%$ is likely because at this point the three phases (*Cm*, *P*4*mm*, and *Amm*2) have similar energies, and macroscopically the average of *P*4*mm* and *Amm*2 also give rise to the *Cm* phase. On the other hand,

when $s > 1\%$, $P4mm$ is no longer an option as its energy becomes much higher than the other two. Because the energy difference between $Amm2$ and Cm continues to be smaller with the misfit strain, the Cm phase can only exist at low temperatures, and eventually disappears. The Cm phase rarely appear in pure perovskites, whether it is epitaxially strained or not, and $SnTiO_3$ seems to be an important exception. Figure 4(b) plots the polarization *versus* the misfit strain for the Cm phase, which is similar to the results obtained in Ref. [9], showing that P_z increases while $P_{x,y}$ decreases with increasing epitaxial strain. We finally note that, despite many attempts, no structural phases involving AFD tilting were found to be at the ground state. For $0\% < s < 5\%$, structural phases without AFD are consistently more stable in terms of energy.

4. Discussion

In Section 3 we have shown that $SnTiO_3$ has $P4mm$, $Amm2$, and Cm phases under different conditions. However, it is hard to prove that $SnTiO_3$ can only has these three phases for the misfit strain we have investigated. This point is further discussed below in Subsection 4.1. Moreover, we will compare the MC results to direct *ab initio* results and focus on the Cm phase in Subsection 4.2.

4.1. Seeking new phases

Phonon calculations have shown that for $SnTiO_3$ the AFD-related modes are also unstable.[20] Considering this fact, it is rather surprising that the MC simulation results are unable to identify new phases involving oxygen octahedron tilting, which is a pity and an important lesson.

We had intentionally played with the coefficients in the effective Hamiltonian and performed additional MC simulations to suggest new phases involving AFD. The simulations results indeed generated a few AFD-related candidates (*e.g.*, the $Ima2$, $Imma$, and $I4cm$ phases). However, direct *ab initio* calculations do not validate them as energy ground states, which is consistent with the fact that Parker *et al.* did not propose any AFD related phases although their calculations have shown strong AFD instability.[20] Therefore, our results strongly suggest that $SnTiO_3$ may not have AFD-related phases as ground state for the misfit strain of $s < 5\%$.

The fact that AFD-related phases do not appear is most likely to be due to the strong competition from the polar local mode, which is responsible for the polarization in $SnTiO_3$. For ferroelectric materials, AFD is usually adverse to the development of polarization. One term in the effective Hamiltonian specifically represents such an effect, which is $D\boldsymbol{\omega}^2\boldsymbol{u}^2$,[58] where the sign of the coupling coefficient (D) will determine how strong the competition (or in rare cases the cooperation) between the local mode $\boldsymbol{u}$ (related to polarization) and $\boldsymbol{\omega}$ (related to AFD). In $SnTiO_3$, the ferroelectric local mode (which is responsible for the $P4mm$, $Amm2$, and Cm phases) apparently dominates the system.

4.2. The *Cm* phase

The results from *ab initio* computations in Fig. 4 show that the Cm phase has the lowest energy beyond $s = 0$ among the $P4mm$, Cm, and $Amm2$ phases. Meanwhile, the phase diagram obtained from MC simulations shows that $SnTiO_3$ exhibits the Cm phase in a much smaller misfit strain range. The most likely reason of this discrepancy is that the lone pair on Sn^{2+} can cause an extra out-of-plane polarization that is not well-accounted for in the effective Hamiltonian, where the polarization is closely related to the Γ-point (of the cubic phase) unstable polar mode.[32,33]

For $SnTiO_3$ that mode is $u_{x,y,z} = (\xi_{Sn}, \xi_{Ti}, \xi_{O_\parallel}, \xi_{O_\perp}, \xi_{O_\perp}) = (0.534, 0.169, -0.411, -0.508, -0.508)$ (normalized), which approximately represents the ion displacements in $SnTiO_3$ and specifies how spontaneous polarization develops. However, some anomaly happens for $SnTiO_3$ as can be seen from the direct *ab initio* computation. For instance, at $s = 1\%$, along the z direction the ion displacements are $u'_z = (0.847, 0.352, -0.049, -0.27, -0.27)$ while along the x, y directions, $u'_{x,y} = (0.781, 0.259, -0.150, -0.387, -0.387)$. It is important to note that u' has a much larger weight on Sn^{2+}, which is not reflected in u. In fact, this is a known issue during the development of the effective Hamiltonian approach as discussed in Ref. [38] where it was pointed out that for $KNbO_3$ and $PbTiO_3$ there is large difference between the experimental and theoretical local modes. Here, $SnTiO_3$ has the same problem while the difference between $PbTiO_3$ and $SnTiO_3$ is discussed in detail in Ref. [59]. In principle, for $SnTiO_3$ it is possible to tune the values of u (or adding an extra polar mode) in the effective Hamiltonian to alleviate or fix this issue. However, this move will involve many more cumbersome calculations of coupling coefficients, making the approach more complicated. This issue again shows the complexity of $SnTiO_3$ despite its simple composition.

5. Conclusion

Using effective Hamiltonian-based MC simulations, we have investigated epitaxially strained $SnTiO_3$, found their structural phases at finite temperatures, and obtained its phase diagram with respect to temperature and misfit strain. The phase diagram of $SnTiO_3$ turns out to be rather complicated, containing two triple points and boundaries that separate ferroelectric phases. These special features provide unique opportunities to design novel high-performance ferroelectric materials containing $SnTiO_3$, in which the rarely seen Cm phase can exist. In addition, while phonon calculation has shown that AFD related modes are unstable,[20] no AFD-related structural phases were found in our simulations, which is likely to be due to the strong competition from unstable polar modes.

References

[1] Xu R J, Liu S, Grinberg I, Karthik J, Damodaran A R, Rappe A M and Martion L W 2015 *Nat. Mater.* **14** 79

[2] Jaffe B, Cook W R and Jaffe H 1971 *Piezoelectric Ceramics* (London: Academic)

[3] Saito Y, Takao H, Tani T, Nonoyama T, Takatori K, Homma T, Nagaya T and Nakamura M 2004 *Nature* **432** 84

[4] Liu W F and Ren X B 2009 *Phys. Rev. Lett.* **103** 257602

[5] Jaffe B, Roth R S and Marzullo S 1954 *J. Appl. Phys.* **25** 809

[6] Zeng Y, Bokov A A, Wang D, Xiang F and Hong W 2018 *Ceram. Inter.* **44** 17548

[7] Wessels B W 2007 *Ann. Rev. Mater. Res.* **37** 659

[8] Ramesh R and Spaldin N A 2007 *Nat. Mater.* **6** 21

[9] Hwang H Y, Iwasa Y, Kawasaki M, Keimer B, Nagaosa N and Tokura Y 2012 *Nat. Mater.* **11** 103

[10] Yamada H, Ogawa Y, Ishii Y, Sato H, Kawasaki M, Akoh H and Tokura Y 2004 *Science* **305** 646

[11] Ohtomo A and Hwang H Y 2004 *Nature* **427** 423

[12] Spaldin N A and Fiebig M 2005 *Science* **309** 391

[13] Wang L, Ju S, You L, Qi Y J, Guo Y W, Ren P, Zhou Y and Wang J L 2015 *Sci. Rep.* **5** 18707

[14] He F Z, Wells B O, Ban Z G, Alpay S P, Grenier S, Shapiro S M, Si W D, Clark A and Xi X X 2004 *Phys. Rev. B.* **70** 235405

[15] Jiang Z J, Zhang R Z, Wang D W, Sichuga D, Jia C L and Bellaiche L 2014 *Phys. Rev. B* **89** 214113

[16] Wu J, Xiao D and Zhu J 2015 *Chem. Rev.* **115** 2559

[17] Armiento R, Kozinsky B, Fornari M and Ceder G 2011 *Phys. Rev. B* **84** 014103

[18] Matar S, Baraille I and Subramanian M 2009 *Chem. Phys.* **355** 43

[19] Lebedev A I 2009 *Phys. Solid State* **51** 362

[20] Parker W D, Rondinelli J M and Nakhmanson S M 2011 *Phys. Rev. B* **84** 245126

[21] Xie Y H, Yin S, Hashimoto T, Kimura H and Sato T 2009 *J. Mater. Sci.* **44** 4834

[22] Ren P R, Liu Z C, Wang Q, Peng B L, Ke S M, Fan H Q and Zhao G Y 2017 *Sci. Rep.* **7** 6693

[23] Bennett J W, Grinberg I, Davies P K and Rappe A M 2011 *Phys. Rev. B* **83** 144112

[24] Suzuki S, Honda A, Iwaji N, Higai S, Ando A, Takagi H, Kasatani H and Deguchi K 2012 *Phys. Rev. B* **86** 060102

[25] Laurita G, Page K, Suzuki S and Seshadri R 2015 *Phys. Rev. B* **92** 214109

[26] Agarwal R, et al. 2018 *Phys. Rev. B* **97** 054109

[27] Taib M F M, Yaakob M K, Hassan O H and Yahya M Z 2013 *Integr. Ferroelectr.* **142** 119

[28] Taib M F M, Yaakob M K, Badrudin F W, Kudin T I T, Hassan O H and Yahya M Z A 2014 *Integr. Ferroelectr.* **459** 134

[29] Uratani Y, Shishidou T and Oguchi T 2008 *Jpn. J. Appl. Phys.* **47** 7735

[30] Zhang R Z, Wang D W, Li F, Ye H J, Wei X Y and Xu Z 2013 *Appl. Phys. Lett.* **103** 062905

[31] Zhang R Z, Wang D W, Zhu X H, Ye H J, Wei X Y and Xu Z 2014 *J. Appl. Phys.* **116** 174101

[32] Zhong W, Vanderbilt D and Rabe K M 1994 *Phys. Rev. Lett.* **73** 1861

[33] Zhong W, Vanderbilt D and Rabe K M 1995 *Phys. Rev. B* **52** 6301

[34] H J Ye, Wang D W, Jiang Z J, Cheng S and Wei X Y 2016 *Acta Phys. Sin.* **65** 237101 (in Chinese)

[35] Nishimatsu T, Iwamoto M, Kawazoe Y, and Waghmare U V 2010 *Phys. Rev. B* **82** 134106

[36] Vanderbilt D and Cohen M H 2001 *Phys. Rev. B* **63** 094108

[37] Kornev I A, Bellaiche L, Janolin P E, Dkhil B and Suard E 2006 *Phys. Rev. Lett.* **97** 157601

[38] King-Smith R D and Vanderbilt D 1994 *Phys. Rev. B* **49** 5828

[39] Jiang Z J, Xu B, Li F, Wang D, and Jia C L 2015 *Phys. Rev. B* **91** 014105

[40] Al-Barakaty A, Prosandeev S, Wang D, Dkhil B, Bellaiche L 2015 *Phys. Rev. B* **91** 214117

[41] Gonze X, Beuken J M, Caracas R, Detraux F, Fuchs M, Rignanese G M, Sindic L, Verstraete M, Zerah G, Jollet F, Torrent M, Roy A, Mikami M, Ghosez P, Raty J Y and Allan D C 2002 *Comput. Mater. Sci.* **25** 478

[42] Perdew J P and Wang Y 1992 *Phys. Rev. B* **45** 13244

[43] Blochl P E 1994 *Phys. Rev. B* **50** 17953

[44] Garrity K F, Bennett J W, Rabe K M and Vanderbilt D 2014 *Comput. Mater. Sci.* **81** 446

[45] Monkhorst H J and Pack J D 1976 *Phys. Rev. B* **13** 5188

[46] Liu K, Fan H Q, Ren P R and Yang C 2010 *J. Alloys Compd.* **509** 1901

[47] Zhang J X, He Q, Trassin M, *et al.* 2011 *Phys. Rev. Lett.* **107** 147602

[48] Zhang N, Yokota H, Glazer A M, Ren Z, Keen D A, Keeble D S, Thomas P A and Ye Z G 2014 *Nat. Commun.* **5** 5231

[49] Lu X, Zheng L, Li H and Cao W 2015 *J. Appl. Phys.* **117** 134101

[50] Liu H, Chen J, Fan L, Ren Y, Pan Z, Lalitha K V, Rdel J and Xing X 2017 *Phys. Rev. Lett.* **119** 017601

[51] Schlom D G, Chen L Q, Eom C B, Rabe K M, Streiffer S K and Triscone J M 2007 *Ann. Rev. Mater. Res.* **37** 589

[52] Xue D Z, Zhou Y M, Bao H X, Gao J H, Zhou C and Ren X B 2011 *Appl. Phys. Lett.* **99** 122901

[53] Liu L J, Zheng S Y, Huang Y M, Shi D P, Wu S S, Fang L, Hu C Z and Elouadi B 2012 *J. Phys. D: Appl. Phys.* **45** 295403

[54] Guo R, Cross L E, Park S E, Noheda B, Cox D E and Shirane G 2000 *Phys. Rev. Lett.* **84** 5423

[55] Cox D E, Noheda B, Shirane G, Uesu Y, Fujishiro K and Yamada Y 2001 *Appl. Phys. Lett.* **79** 400

[56] Liu L J, Huang Y M, Li Y H, Fang L, Dammak H, Fan H Q and Thi M P 2012 *Mater. Lett.* **68** 300

[57] Wada S, Suzuki S, Noma T, Suzuki T, et al. 1999 *Jpn. J. Appl. Phys.* **38** 5505

[58] Wang D W, *et al.*, 2011 *Phys. Rev. Lett.* **107** 175502

[59] Pitike K C, Parker W D, Louis L and Nakhmanson S M 2015 *Phys. Rev. B* **91** 035112